AIP | Applied Physics Letters

Highly efficient indium tin oxide-free organic photovoltaics using inkjet-printed silver nanoparticle current collecting grids

M. Neophytou, F. Hermerschmidt, A. Savva, E. Georgiou, and S. A. Choulis

Citation: Appl. Phys. Lett. **101**, 193302 (2012); doi: 10.1063/1.4765343
View online: http://dx.doi.org/10.1063/1.4765343
View Table of Contents: http://apl.aip.org/resource/1/APPLAB/v101/i19
Published by the AIP Publishing LLC.

Highly efficient indium tin oxide-free organic photovoltaics using inkjet-printed silver nanoparticle current collecting grids

M. Neophytou, F. Hermerschmidt, A. Savva, E. Georgiou, and S. A. Choulis[a)]
Molecular Electronics and Photonics Research Unit, Department of Mechanical Engineering and Materials Science and Engineering, Cyprus University of Technology, 3036 Limassol, Cyprus

(Received 2 May 2012; accepted 18 October 2012; published online 5 November 2012)

We report an in-depth investigation of an inkjet-printed silver (Ag) nanoparticle grid combined with poly(3,4-ethylenedioxythiophene):poly(styrenesulfonate) (PEDOT:PSS) of different conductivities as an alternative to an indium tin oxide (ITO)-based transparent anode for organic solar cell applications. The reported measurements revealed higher transparency of the inkjet-printed Ag nanoparticle-based grid when compared to different thicknesses of ITO on glass substrates. Based on the proposed current collecting grid, a record power conversion efficiency of 2% is achieved for ITO-free organic solar cells. © *2012 American Institute of Physics*. [http://dx.doi.org/10.1063/1.4765343]

The field of organic photovoltaics (OPV) has been attracting great scientific attention over the last few years. New fields of applications are feasible as OPV are lightweight, flexible, and have the potential for truly low fabrication cost. At present, so-called bulk heterojunction structures based on blends of a conjugated polymer as electron donor and a soluble fullerene derivative as acceptor represent the OPV material system with the highest power conversion efficiency (PCE) reported until now. Recent developments include power conversion efficiencies up to 9%,[1] durability of 1 year under real environmental conditions,[2] accelerated lifetime test results indicating longer OPV lifetimes,[3] and proof of concept for high throughput fabrication using printing and spray coating technologies.[4–9]

Based on the recent progress on power conversion efficiency, lifetime and processing, one of the issues which needs to be urgently addressed is materials cost.[10] Cost reduction is considered as the next important milestone for OPVs and replacement of high cost materials on the OPV device structure is critical for the future technological progress of OPVs. Most of the high performance OPV devices reported in the literature use rigid and stiff indium tin oxide (ITO) as the transparent electrode, which is deposited by sputtering at high vacuum and temperatures, prohibiting further reduction in fabrication cost. ITO is the most expensive component of the OPV device structure and the need for inexpensive alternative transparent electrodes is imminent.

Ideally, transparent conductive oxides (TCOs) exhibit high optical transparency while simultaneously being highly conductive so that electric charge carrier extraction can be evenly distributed.[11] Many research groups have reported sputtered or thermally evaporated alternative to ITO such as fluorine doped tin oxide (FTO),[12] which has high air and chemical stability and is less expensive than ITO. Furthermore, lithographically deposited metal grids,[13] single-walled carbon nanotubes,[14,15] ultra-thin graphene layers,[16] and oxygenated nano-crystalline diamonds[17] are considered as alternative paths to follow for ITO-free organic solar cells. A further promising alternative to these are PEDOT:PSS derivatives,[18–21] a conductive transparent buffer layer which has been extensively studied, but as it exhibits significantly lower conductivity values than those obtained with ITO, the overall device performance is limited. Low conductivity results in high sheet resistance, thus decreasing the capability of the PEDOT:PSS anode to extract charge species efficiently in those cases that it is not combined with ITO. In order to diminish resistance losses, inkjet printed Ag-nanoparticle grid lines have been integrated with PEDOT:PSS and ITO-free OPVs with a PCE of 1.47% have been recently reported.[22] In this paper, we report an in-depth investigation of an inkjet-printed silver nanoparticle grid combined with different conductivity PEDOT:PSS. We have achieved an ultimate control of the design requirements of current collecting grids based on the proposed inkjet-printing process to accurately control the uniformity and dimensions of the silver nanoparticle based grid. The performed measurements revealed higher transparency of the printed Ag-grid when compared to different thicknesses of ITO. As a result, a record power conversion efficiency of 1.96% is reported for ITO-free organic solar cells using the combination of PEDOT:PSS/inkjet printed nanoparticles based current collecting grid.

The applied experimental procedure is as follows: on top of a common glass substrate Ag nanoparticle ink purchased from SunChemical was inkjet-printed with a Fujifilm Dimatix 2832 series printer. A 10 pl cartridge was used and various conditions and deposition parameters were optimized in such a way that the desired line height and width was achieved. Inkjet printers deploy drop-on-demand (DoD) technology and by altering parameters such as drop spacing the user may control printed grid line thickness. Ink viscosity was manipulated using different cartridge temperatures, so that improved droplet wettability on the glass substrate was achieved. Printed grid lines were fully covered with doctor bladed PEDOT:PSS layers of different conductivities. Layers were thermally treated at 100 °C for 20 min to remove residual solvent. Above these layers, a 1:0.8 by weight ratio

[a)]Author to whom correspondence should be addressed. Electronic mail: stelios.choulis@cut.ac.cy.

(w:w) of P3HT:PCBM was doctor-bladed to achieve a thickness of 280 nm. The top electrode, 100 nm aluminium (Al), was thermally evaporated inside a nitrogen-filled glovebox and the devices were thermally annealed for 15 min at 140 °C. Composite materials of the active layer blend were diluted separately overnight in chlorobenzene and mixed one hour prior to deposition. The photovoltaic active area is defined as cathode and anode overlapping, and for this reason an evaporation shadow mask was used. The device area was measured to be 9 mm^2. The device structure is schematically depicted in Figure 1. For comparison, reference devices of pre-structured ITO substrates were fabricated along with the grid line layers under identical processing conditions.

As instructed by the manufacturer of the Ag ink, a sintering process is needed so that the printed lines achieve optimum conductivity and film properties. A mirror-like appearance (indicating solid silver formation) was visible even after the printed grid lines were sintered for less than one minute at 140 °C on a hot plate. Nonetheless, further exposure of up to 20 min was needed to ensure that no residual solvent of the Ag nanoparticle ink was causing defects at the evaporated metal cathode. These defects, shown in Figure 2(a), are visible to the naked eye as burst bubbles and are in the range of a few micrometers. Indications that the PEDOT:PSS layer was also damaged were observed and extracted data have shown to decrease device performance.

As will be discussed later in the text, the line width and height of the inkjet-printed silver nanoparticle current collecting grid are co-dependent. By varying the deposition temperature, the solvent evaporation rate is altered. At high temperature, a so-called coffee-ring effect[23] (solute buildup on one area, leaving a distinct ring shape upon evaporation) was observed and influenced each line formation. Due to the increased evaporation rate, solvent from the edges of the line was rapidly depleted. In order to replenish the loss, solvent from the center of the line created an outward flow. Shifted nanoparticles were mounted up at the droplet's edges and resulted in an M-shape line formation.[24] Randomly dispersed spike-type shapes of up to 400 nm in some rare cases penetrated the deposited layers, shunting the device. Lack of printed line homogeneity due to coffee-ring line formation could lead to non-uniform conductivity, thus increasing series resistance in the OPV device performance parameters. Therefore, all efforts were made to achieve undistorted line shapes. Figure 2(b) shows the spikes observed even in an optimized printed line. However, the height of those spikes is only a few tens of nanometers higher than the overall height of the line.

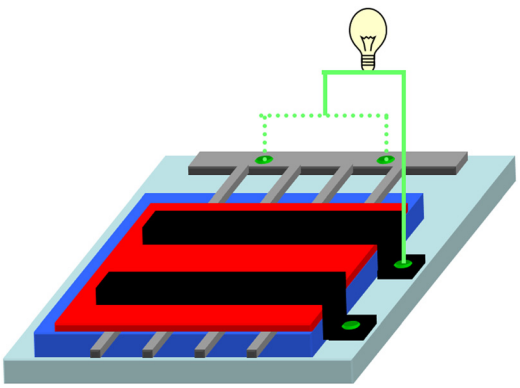

FIG. 1. Representation of ITO-free device structure. The silver grid lines (grey) are deposited onto a glass substrate, followed by PEDOT:PSS (blue) and the active layer (red). The Al cathode (black) is thermally evaporated on top.

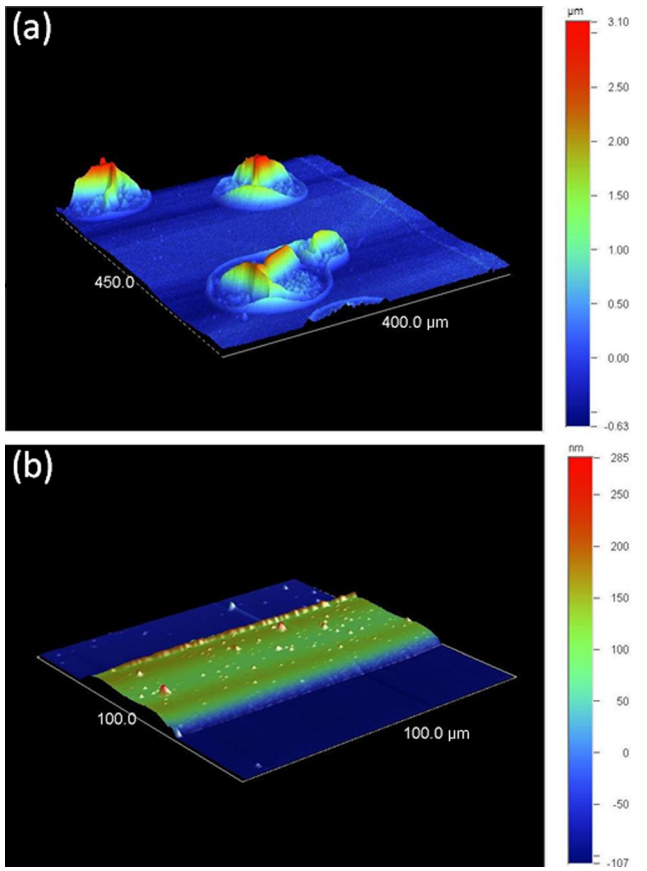

FIG. 2. (a) Surface mapping image showing micron-sized bubbles formed on deposited grid lines where the solvent has not evaporated sufficiently. (b) Surface mapping image of an optimized printed line. The overall height of the line is in the region of 190–210 nm, with the spike-type shapes showing as more prominent points.

To ensure increased charge carrier selective collection through the Ag grids, they have to be entirely covered with PEDOT:PSS. In order to do so, PEDOT:PSS films should be deposited which are thicker than the printed line height. However, despite the fact that increased thickness results in reduced resistivity values of the PEDOT:PSS films, significant transparency losses occur. In order to avoid additional losses, a balance between these two parameters of resistivity and transparency has to be achieved.

As a general rule, an optimized grid structure should allow maximum visible light to pass through and at the same time ensure uniform charge carrier extraction from the entire active area of the photovoltaic cell. Grid lines with small width and height were aimed for in an effort to avoid any undesirable shadow effects. While, the width decreases, increased height will be obtained, as the same amount of material from the 10 pl droplet will be collected in a smaller area. Various drop spacing and deposition temperatures were tested. Optimum combination of these two parameters resulted in a line of 46 μm width and 200 $\pm$ 10 nm height. This is significantly thinner than reported elsewhere,[22]

allowing for more light to reach the P3HT:PCBM active layer part of the OPV device structure. Transmission measurements were therefore carried out to ascertain the positive effects of such a thin grid line architecture.

Transmittance measurements were performed with inkjet-printed silver grid and different thickness ITO sputtered on glass substrates, as shown in Figure 3. Non-coated glass substrates were also used for comparison. The silver nanoparticle inkjet printed grids showed particularly high transmittance (~92%) in the range of the absorption maxima of the P3HT:PCBM active layer, which are between 490 and 560 nm. The grids with 46 μm width were also compared with ones of 49 μm width. Both types resulted in higher than 90% transmittance throughout the visible spectrum and one could suggest that they are suitable for broader absorption material systems as well.

To investigate the effect of PEDOT:PSS conductivity on the overall device performance of ITO-free OPVs using inkjet-printed silver nanoparticle current collecting grids, Clevios P VP AL 4083 and Clevios PH, with conductivity of 0.002 S/cm and 10 S/cm, respectively,[21] were used as electron blocking and hole transporting buffer layers on the ITO-free OPV device structure. Both dispersions were diluted with isopropanol in a ratio of 1:3.2 in order to reduce the surface tension of pristine PEDOT:PSS. Four lines of a silver nanoparticle current collecting grid with 46 μm width and ~200 nm height were printed on glass substrates. The pitch size (the horizontal distance of one line from another) was set at 700 μm and no line was printed at the edges of the OPV device structure to avoid leakage current. Total coverage of the cells with inkjet printed Ag nanoparticle grid lines was 6.2%. We note that ITO-free OPV devices with fewer number of lines were also fabricated but charge carrier collection was significantly reduced.[25]

Uneven current collection distribution increased bimolecular recombination. Excitons which dissociated away from the Ag grid's position could not be extracted and recombined. This was manifested in reduced shunt resistance (R_{sh}) on current density-voltage characteristics (J/V) that for simplicity are not shown here. Evidently, fewer silver lines did not reduce the PEDOT:PSS resistivity and resulted in high series resistance (R_s) as well. Figures 4(a) and 4(b) show J/V characteristics under dark (a) and under illumination (b) of ITO-free OPVs with 46 μm width and ~200 nm height Ag current collecting grids and reference ITO-based OPVs. OPV device performance characteristics were measured using a calibrated Newport 92250 A solar simulator, under 1 sun (100 mW/cm^2) illumination.

Current density-voltage characteristics were measured for both PEDOT:PSS with embedded Ag nanoparticle grids. For comparison, reference devices with ITO electrodes were also fabricated and measured. Active layer and evaporated metal cathode were deposited under identical conditions for both architectures. The optimized process for reference cells resulted in higher overall device performance with PCE reaching 3%. Both PEDOT:PSS types, regardless of conductivity, exhibited a good balance of transmittance and resistance at a layer thickness of around 250 nm as shown by relatively high J_{sc} values. A phase separation of conductive PEDOT-rich clusters with insulating PSS-rich edges are reported after film formation. Higher PSS composite in the dispersion only resulted in films with higher resistivity.[26] When replacing the ITO anode with a silver grid and Clevios

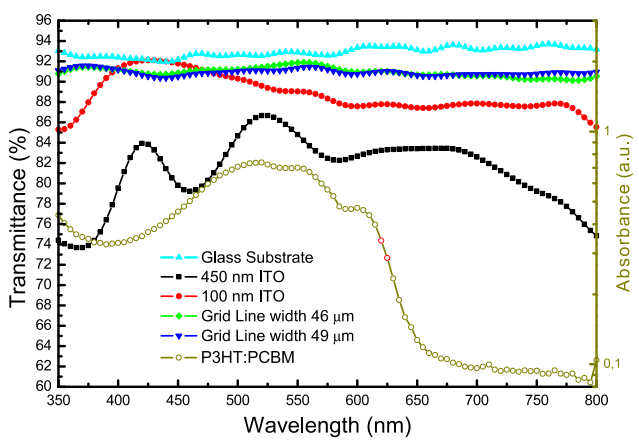

FIG. 3. Optical transmittance of glass substrates with various surface coverings. The transmittance of the Ag grid lines was compared to 100 nm and 450 nm of ITO coverage as well as a reference. Both grid line widths provide >90% transmittance. P3HT:PCBM absorbance is included for comparison (open circles).

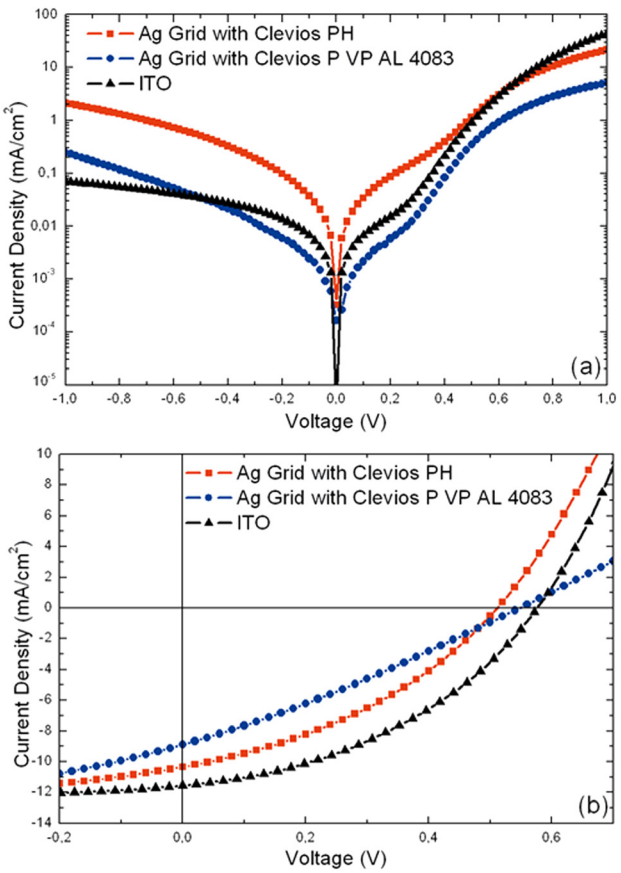

FIG. 4. (a) Effect of PEDOT:PSS conductivity on device performance in dark conditions. PEDOT:PSS with 0.002 S/cm conductivity (blue circles) exhibited higher R_s mainly due to the higher PSS concentration. When compared to the reference structure (black triangles), both devices showed high carrier injection at negative and low positive bias, which is most likely caused by spike-like shapes in the printed line. (b) Effect of PEDOT:PSS conductivity on device performance in light conditions. Despite the fact that loss mechanisms dominated device performance for both ITO-free architectures, a PCE of 1.96% was achieved.

TABLE I. Photovoltaic parameters of devices using inkjet-printed silver (Ag) nanoparticle grid combined with alternative PEDOT:PSS anodes and reference ITO-based organic solar cells for comparison.

Device anode	V_{oc} [mV]	J_{sc} [mA/cm^2]	FF [%]	PCE [%]
Clevios P VP AL 4083/Ag	548	8.90	28.3	1.38
Clevios PH/Ag	510	10.35	36.8	1.96
ITO	570	11.55	45.1	3.04

P VP AL 4083, where the PEDOT:PSS ratio is 1:6 (w/w), series resistance as shown at +1 V (see Figure 4) dominated the overall device performance. According to Ohm's law, in open circuit conditions, no reduction in V_{oc} is expected due to R_s and only FF and J_{sc} values are negatively affected, resulting in 28.3% and 8.9 mA/cm^2, respectively. Generated power in the fourth quadrant is consumed so that the energetic barrier of the increased resistance is overcome.

Improved FF values of around 37% are obtained for devices with more conductive hole transporting layers. Charge carrier transportation and collection are enhanced due to better electrical properties of the Clevios PH PEDOT:PSS. At the same time, better ohmic contacts between the interfaces are formed. Some losses in V_{oc} in the range of 510 mV are mainly attributed to increased dark current density values in the negative and low positive bias for these devices. Shunt resistance was reduced as a result of charge carrier bimolecular recombination and this could only suggest that one of the electrodes lacks selective charge extraction. As all other layers for the reference and ITO-free devices were deposited at identical conditions and parameters, it was reasonable to assume that losses could be attributed to the Ag grid. Selectivity is to some extent reduced as presumably the Ag spikes have penetrated the PEDOT:PSS film and collect both electrons and holes. Fabricated devices with PEDOT:PSS of 10 S/cm conductivity resulted in a power conversion efficiency of 1.96%. This is among the highest PCE obtained from unmodified PEDOT:PSS/inkjet printed Ag grid ITO-free anodes reported in the literature. All device parameters are summarized in Table I.

It is clear that in both PEDOT:PSS/Ag grid anode devices further optimization of line width, height, and pitch size is needed in order to maximize carrier transportation and collection.

In summary, inkjet printing facilitates mass production organic solar cell fabrication. Brittle and expensive ITO can be efficiently replaced by Ag grid lines embedded into conductive PEDOT:PSS films. We have demonstrated that inkjet printed Ag grid lines provide high transparency throughout the entire visible spectrum. For low roughness grid lines, the coffee-ring effect can be avoided with the optimum combination of drop spacing and deposition temperature. Optimum line width was found to be 46 μm so that shadow effects were minimized. Higher conductivity PEDOT:PSS formulations are needed in order to further reduce line height and transmittance losses. A record PCE in the range of 2% was achieved for ITO-free organic solar cells using the combination of PEDOT:PSS/inkjet printed nanoparticles based current collecting grids, but there is still a long way to go towards fully sustainable inexpensively produced solar cells.

This work was co-funded by the European Regional Development Fund and the Republic of Cyprus through the Research Promotion Foundation (Strategic Infrastructure Project NEA ΥΠΟΔΟΜΗ/ΣΤΡΑΤΗ/0308/06).

[1]M. A. Green, K. Emery, Y. Hishikawa, and W. Warta, Prog. Photovoltaics **20**, 12 (2012).
[2]A. Hauch, P. Schilinski, S. A. Choulis, R. Childers, M. Biele, and C. J. Brabec, Sol. Energy Mater. Sol. Cells **92**, 727 (2008).
[3]C. H. Peters, I. T. Sachs-Quintana, J. P. Kastrop, S. Beaupre, M. Leclerc, and M. D. McGehee, Adv. Energy Mater. **1**, 491 (2011).
[4]C. N. Hoth, S. A. Choulis, P. Schilinsky, and C. J. Brabec, Adv. Mater. **19**, 3973 (2007).
[5]C. N. Hoth, P. Schilinsky, S. A. Choulis, and C. J. Brabec, Nano Lett. **8**, 2806 (2008).
[6]C. N. Hoth, R. Steim, P. Schilinsky, S. A. Choulis, S. F. Tedde, O. Hayden, and C. J. Brabec, Org. Electron. **10**, 587 (2009).
[7]M. Neophytou, W. Cambarau, F. Hermerschmidt, C. Waldauf, C. Christodoulou, R. Pacios, and S. A. Choulis, Microelectron. Eng. **95**, 102 (2012).
[8]M. M. Voigt, R. C. I. Mackenzie, C. P. Yau, P. Atienzar, J. Dane, P. E. Keivanidis, D. D. C. Bradley, and J. Nelson, Sol. Energy Mater. Sol. Cells **95**, 731 (2011).
[9]F. C. Krebs, Sol. Energy Mater. Sol. Cells **93**, 394 (2009).
[10]C. J. M. Emmot, A. Urbina, and J. Nelson, Sol. Energy Mater. Sol. Cells **97**, 14 (2012).
[11]D. S. Hecht, L. Hu, and G. Irvin, Adv. Mater. **23**, 1482 (2011).
[12]A. Andersson, N. Johansson, P. Broms, N. Yu, D. Lupo, and W. R. Salaneck, Adv. Mater. **10**, 859 (1998).
[13]M. G. Kang, M. S. Kim, J. S. Kim, and L. J. Guo, Adv. Mater. **20**, 4408 (2008).
[14]A. A. Green and M. C. Hersam, Nano Lett. **8**, 1417 (2008).
[15]J. L. Blackburn, T. M. Barns, M. C. Beared, Y. Kim, R. C. Tenent, T. J. McDonald, B. To, T. J. Coutts, and M. J. Heben, ACS Nano **2**, 1266 (2008).
[16]L. G. de Arco, Y. Zhang, C. W. Schlenker, K. Ryu, M. E. Thompson, and C. W. Zhou, ACS Nano **4**, 2865 (2010).
[17]C. H. Y. X. Lim, Y. L. Zhong, S. Janssens, M. Nesladek, and K. P. Loh, Adv. Funct. Mater. **20**, 1313 (2010).
[18]T. Aernouts, P. Vanlaeke, W. Geens, J. Poortmans, P. Heremans, S. Borghs, R. Mertens, R. Andriessen, and L. Leenders, Thin Solid Films **451**, 22 (2004).
[19]S. I. Na, S. S. Kim, J. Jo, and D. Y. Kim, Adv. Mater. **20**, 4061 (2008).
[20]J. Huang, X. Wang, Y. Kim, A. J. de Mello, D. D. C. Bradley, and J. C. de Mello, Phys. Chem. Chem. Phys. **8**, 3904 (2006).
[21]X. Wang, T. Ishwara, W. Gong, M. Campoy-Quiles, J. Nelson, and D. D. C. Bradley, Adv. Funct. Mater. **22**, 1454 (2012).
[22]Y. Galagan, B. Zimmermann, E. W. C. Coenen, M. Jørgensen, D. M. Tanenbaum, F. C. Krebs, H. Gorter, S. Sabik, L. H. Slooff, S. C. Veenstra, J. M. Kroon, and R. Andriessen, Adv. Energy Mater. **2**, 103 (2012).
[23]M. Layani, M. Gruchko, O. Milo, I. Balberg, D. Azulay, and S. Magdassi, ACS Nano **3**, 3537 (2009).
[24]Y. Jang, J. Jo, and D. S. Kim, J. Polym. Sci., Part B: Polym. Phys. **49**, 1590 (2011).
[25]A. Cheknane, Prog. Photovoltaics **19**, 155 (2011).
[26]U. Lang, E. Muller, N. Naujoks, and J. Dual, Adv. Funct. Mater. **19**, 1215 (2009).